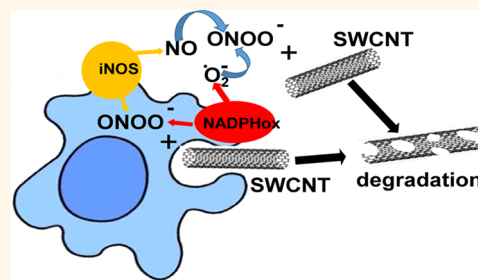


Lung Macrophages “Digest” Carbon Nanotubes Using a Superoxide/Peroxynitrite Oxidative Pathway

Valerian E. Kagan,^{†,‡,*} Alexandr A. Kapralov,^{†,‡} Claudette M. St. Croix,[‡] Simon C. Watkins,[§] Elena R. Kisin,^{||} Gregg P. Kotchey,[†] Krishnakumar Balasubramanian,^{†,‡} Irina I. Vlasova,^{†,‡,¶} Jaesok Yu,[¶] Kang Kim,[¶] Wanji Seo,[†] Rama K. Mallampalli,^{¶,△,▲} Alexander Star,[†] and Anna A. Shvedova^{||}

[†]Center for Free Radical and Antioxidant Health, [‡]Acute Lung Injury Center of Excellence, [§]Departments of Environmental and Occupational Health, [¶]Cell Biology and Physiology, ^{||}Chemistry, and [¶]Medicine, University of Pittsburgh, Pittsburgh, Pennsylvania, United States, [△]Medical Specialty Service Line, Veterans Affairs Pittsburgh Healthcare System, Pittsburgh, Pennsylvania, United States, [¶]Pathology and Physiology Research Branch, Health Effects Lab Division, National Institute for Occupational Safety and Health, Morgantown, West Virginia, United States, and [▲]Research Institute of Physico-Chemical Medicine, Moscow 119495, Russia

ABSTRACT In contrast to short-lived neutrophils, macrophages display persistent presence in the lung of animals after pulmonary exposure to carbon nanotubes. While effective in the clearance of bacterial pathogens and injured host cells, the ability of macrophages to “digest” carbonaceous nanoparticles has not been documented. Here, we used chemical, biochemical, and cell and animal models and demonstrated oxidative biodegradation of oxidatively functionalized single-walled carbon nanotubes *via* superoxide/NO* → peroxynitrite-driven oxidative pathways of activated macrophages facilitating clearance of nanoparticles from the lung.



KEYWORDS: single-walled carbon nanotubes · peroxynitrite · biodegradation · lung

In spite of successful applications of nanoparticles in *experimental* nanomedicine, their advancement into *clinical* trials has been decelerated and challenged by concerns about their potential adverse health effects and unusual biopersistence in the lung, leading to chronic inflammation and potential carcinogenicity and tumor growth.^{1,2} With regard to carbonaceous nanomaterials, the initial observations documented their presence in the lung even one year after inhalation or aspiration exposure.^{3,4} More focused analysis, however, revealed that this was relevant to only long (high aspect ratio) and highly aggregated single-walled carbon nanotubes (SWCNTs) frequently encapsulated in interstitial granulomas.^{5,6} In fact, short (low aspect ratio) and well-dispersed SWCNTs demonstrated markedly accelerated rates of clearance compared with the high aspect ratio aggregated particles.^{6,7} This suggests that short SWCNTs may be taken up by cells, likely inflammatory cells, facilitating their biodegradation.

The chemical degradation of pristine SWCNTs using strong acids and oxidants (such as mixtures of sulfuric acid and hydrogen

peroxide) has been known for quite some time.⁸ SWCNTs can also be degraded by highly reactive hydroxyl radicals (·OH) produced *via* Fenton homolytic cleavage of H₂O₂.⁹ Due to the high oxidative potential (~2.3 V),¹⁰ this reactive species is able to oxidize both pristine and carboxylated SWCNTs. In addition to chemical oxidants, recent work discovered and characterized “mild” enzymatic catalytic pathways for biodegradation of SWCNTs and multiwalled CNTs (MWCNTs).^{11,12} Reactive intermediates of several peroxidases—plant horseradish peroxidase (HRP), inflammatory cells myeloperoxidase (MPO), and eosinophil peroxidase (EPO)—were found to be effective in oxidative biodegradation of CNTs in biochemical models and in cells.^{13,14} Reactive intermediates generated during catalytic cycles of these enzymes, particularly oxoferryl iron (Fe⁴⁺=O), can oxidize a variety of substrates, including CNTs.^{15,16} In addition, the well-documented ability of MPO and EPO to convert halides into strong oxidants—hypochlorous acid (HOCl) and hypobromous acid (HOBr), respectively—contributes to the CNT biodegradation

* Address correspondence to kagan@pitt.edu.

Received for review December 18, 2013 and accepted May 28, 2014.

Published online May 28, 2014
10.1021/nn406484b

© 2014 American Chemical Society

process.^{11,17} Interestingly, biodegradation of CNTs by oxidative metabolism of bacteria accompanied by the formation of multiple products has been considered as a potentially important mechanism in the environment. Genotypic characterizations revealed three microbial species likely involved in degradation of CNTs: *Burkholderia kururiensis*, *Delftia acidovorans*, and *Stenotrophomonas maltophilia*.¹⁸

PMNs (polymorphonuclear leukocytes) have been identified as an inflammatory cell population capable of biodegrading SWCNTs via activation of their powerful pro-oxidant myeloperoxidase-catalyzed pathways.¹³ However, PMNs are short-lived¹⁹ and can define the fate of SWCNTs only within 3 to 4 days after initial exposure.²⁰ In contrast, macrophages may persist over weeks of chronic inflammation elicited by pulmonary exposure to SWCNTs. This characteristic, combined with the known propensities of macrophages to recognize and take up SWCNTs, makes them a very likely candidate cell type that determines the kinetics of SWCNT clearance from the lung. In contrast to PMNs, however, macrophages do not express significant amounts of MPO.^{16,21} Instead, their oxidative metabolism and “digestion” of foreign invaders are driven by highly expressed enzymes producing superoxide ($\text{O}_2^{\bullet-}$)-NADPH oxidase and nitric oxide (NO^{\bullet})-inducible isoform of nitric oxide synthases (iNOS).^{22,23} These two radical species rapidly react to yield a highly potent oxidant, peroxynitrite (ONOO^-), which can effectively modify many types of biomolecules.^{24,25} Here, we report that superoxide/ NO^{\bullet} → peroxynitrite-driven oxidative pathways of macrophages are, indeed, involved in the “digestion” of SWCNTs and their clearance from the lung.

RESULTS

Inhalation or pharyngeal aspiration exposure of mice to SWCNTs triggers a robust inflammatory response whereby the initial sharp accumulation and activation of neutrophils is followed by the expedited recruitment and extended presence of macrophages in the lung.^{20,14} As neutrophils are equipped to “oxidatively kill” bacterial invaders by MPO-driven reactions,^{16,21} they have also been shown to oxidatively partially biodegrade CNTs.^{13,14} Arriving macrophages “clean” the oxidative battlefield by phagocytotic digestion of injured neutrophils and also take up still abundant CNTs. It has been documented that maximal recruitment and accumulation of macrophages in the lungs of w/t and gp91^(phox)^(-/-) mice exposed to a dose of 40 µg of SWCNT/animal—the same dose as the one utilized in the current work—was maximal on day 7 after the exposure.^{20,26} Given that macrophage NADPH oxidase is the major generator of superoxide radicals required for the production of peroxynitrite involved in the SWCNT biodegradation, we chose to conduct our comparative measurements on days 7 and 28, respectively. These considerations were further supported by

our previous characterizations of SWCNTs using Raman microscopy, in which no significant changes were detected between days 1 and 7, whereas a marked decrease of the levels and oxidative modification of carbon nanotubes was detected on days 1 and 28 after the exposure.¹⁴ In addition, our assessments of the SWCNT content using quantitative optical imaging of the lung sections (using the spectral range 750–840 nm selectively absorbed by SWCNTs) did not reveal differences between the volumes occupied by SWCNTs on days 1 and 7 postexposure.¹⁴ On this basis, we reasoned that comparative assessments of the SWCNT contents in the lungs on days 7 and 28 are well justified.

We assessed the SWCNT content in alveolar macrophages of C57BL6 mice using enhanced dark-field microscopy with hyperspectral image analysis by CytoViva.²⁷ We and others have validated the utility of this approach in several published studies.²⁸ Oxidatively functionalized SWCNTs (treated with concentrated $\text{H}_2\text{SO}_4/\text{HNO}_3$ at a ratio of 3:1 at 70 °C for 40 min) have been used in all experiments. As shown in Figure 1, SWCNT-loaded macrophages are readily detectable in both bronchoalveolar lavage (BAL) and lung macrophages of C57BL6 mice on day 7 after pharyngeal aspiration exposure (40 µg/mouse). Quantitatively, at this time point, more than 50% of BAL macrophages and ~12% of lung tissue macrophages are SWCNT-laden (Figure 1A,C,E). Notably, this significant early presence of SWCNTs in macrophages markedly decreased by the 28th day after the exposure, resulting in their counts of ~10–12% and <1% in BAL and the lung, respectively (Figure 1B,D,F).

While redistribution and migration of macrophages might significantly contribute to SWCNT clearance, “digestion” of SWCNTs within macrophages might represent yet another factor of SWCNT disappearance. SWCNTs have been shown to be sensitive to oxidative biodegradation by MPO intermediates and hypochlorous acid generated by neutrophils.^{13,11} A comparably potent oxidant (with a redox potential of +1.4 V²⁹) is peroxynitrite (ONOO^-), which can be generated by macrophages in the reaction of superoxide radicals with nitric oxide (NO^{\bullet}):



It is believed that highly expressed NADPH oxidase and NO synthase are the two suppliers of the reactants for reaction 1, leading to massive peroxynitrite production by activated macrophages. Therefore, we reasoned that ONOO^- might be involved, at least in part, in the macrophage biodegradation of SWCNTs in the lung. To experimentally test this, we compared the content of SWCNTs in lung macrophages on the 28th day after the exposure in wild-type C57BL6 mice with NADPH-oxidase-deficient (gp91^(phox)^(-/-)) mice (Figure 1F). We found that clearance of SWCNTs was ~10-fold less effective in the gp91^(phox)^(-/-) mice vs w/t animals. In

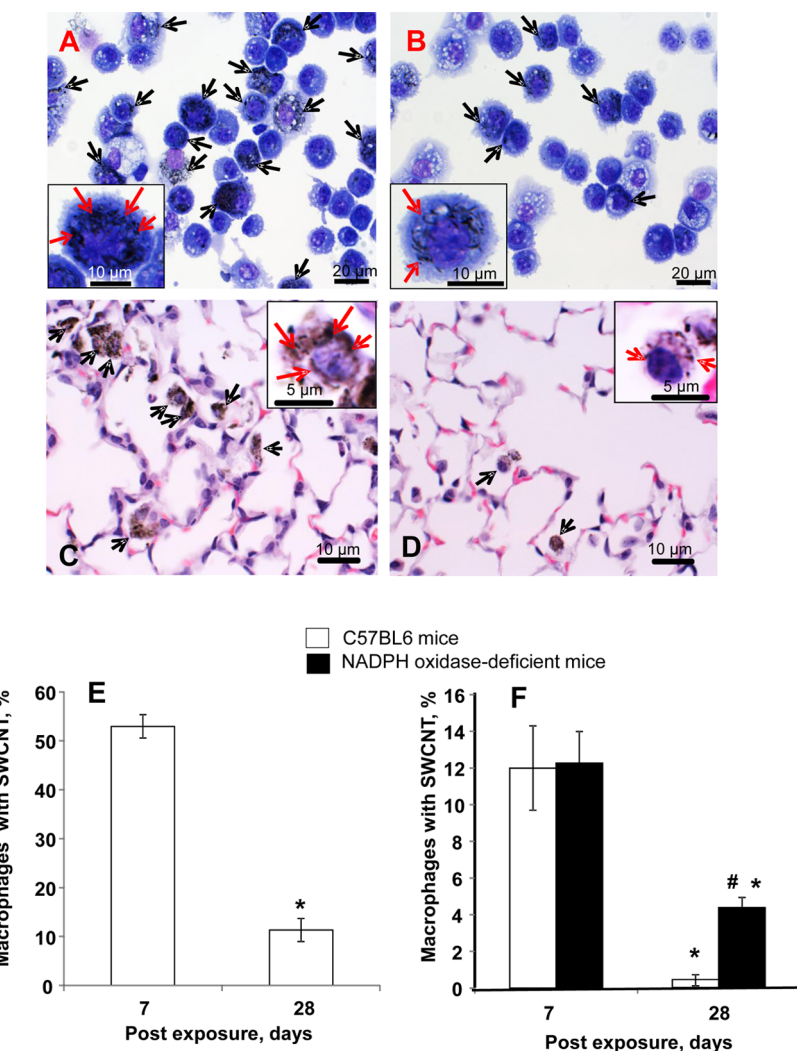


Figure 1. Assessment of the amounts of alveolar macrophages with SWCNTs in BAL (A, B, E) and lung sections (C, D, F) of adult C57BL/6 [$\text{gp91}^{\text{phox}}^{+/+}$] and NADPH-oxidase-deficient [$\text{gp91}^{\text{phox}}^{-/-}$] mice on days 7 and 28 post SWCNT exposure. (A, B, C, D) Representative images of BAL cells (A, B) or lung sections (C, D) of C57BL/6 mice on day 7 (A, C) and day 28 (B, D) after exposure to SWCNTs. Original magnification $60\times$. Arrows show SWCNTs present in individual alveolar macrophages. Inset: Representative BAL/lung macrophages with SWCNTs. (E) Quantitative results of alveolar macrophages with SWCNTs in BAL of C57BL/6 mice. (F) Quantitative results of lung tissue macrophages with SWCNTs in lung sections of C57BL6 and NADPH-oxidase-deficient mice. Results are mean \pm SEM ($n = 5$ mice/group). * $p < 0.05$, vs day 7 post SWCNT exposure; # $p < 0.05$, vs C57BL6 mice on day 28 postexposure.

BAL of NADPH-oxidase-deficient mice, we found similar amounts of SWCNT-loaded macrophages ($\sim 23 \times 10^4$) on both day 7 and 28 after exposure.

To further quantitatively assess the differences in SWCNT clearance between w/t vs NADPH oxidase k/o mice, we performed independent measurements of their content in the lungs using photoacoustic (PA) imaging³⁰ (Figure 2). In wild-type C57BL6 mice, the PA signal intensity from SWCNTs on day 28 (-18.5 ± 5.6 dB) was more than 2-fold lower compared to that on day 7 (-10.6 ± 3.7 dB). In contrast, no significant difference was observed between day 7 (-10.5 ± 5.0 dB) and day 28 (-12.8 ± 4.9 dB) PA signal intensities in NADPH-oxidase-deficient mice.

Given that oxidative potential of superoxide anion radicals (-0.33 V)³¹ is not sufficient for direct oxidative degradation of SWCNT, we concluded that superoxide/

NO* → peroxy nitrite-driven oxidative pathways were involved in the clearance process. To directly assess the ability of macrophages to utilize the superoxide/NO* → peroxy nitrite oxidative system in SWCNT biodegradation, we utilized a model of activated THP-1 macrophages known to generate peroxy nitrite upon stimulation with phorbol 12-myristate 13-acetate (PMA).³² Differential interference contrast (DIC) microscopy revealed that activated (but not quiescent) macrophages engulfed SWCNTs (129 ± 12.7 particles per cell and 2.7 ± 0.2 particles per cell, respectively) (Figure 3). We further applied live cell imaging using hydroxyl radical and peroxy nitrite sensor hydroxyphenyl fluorescein (HPF),³³ which generates a highly fluorescent oxidation product after reaction with peroxy nitrite anions or hydroxyl radicals. Data obtained by live cell imaging demonstrated that naïve THP-1 cells have a weak HPF

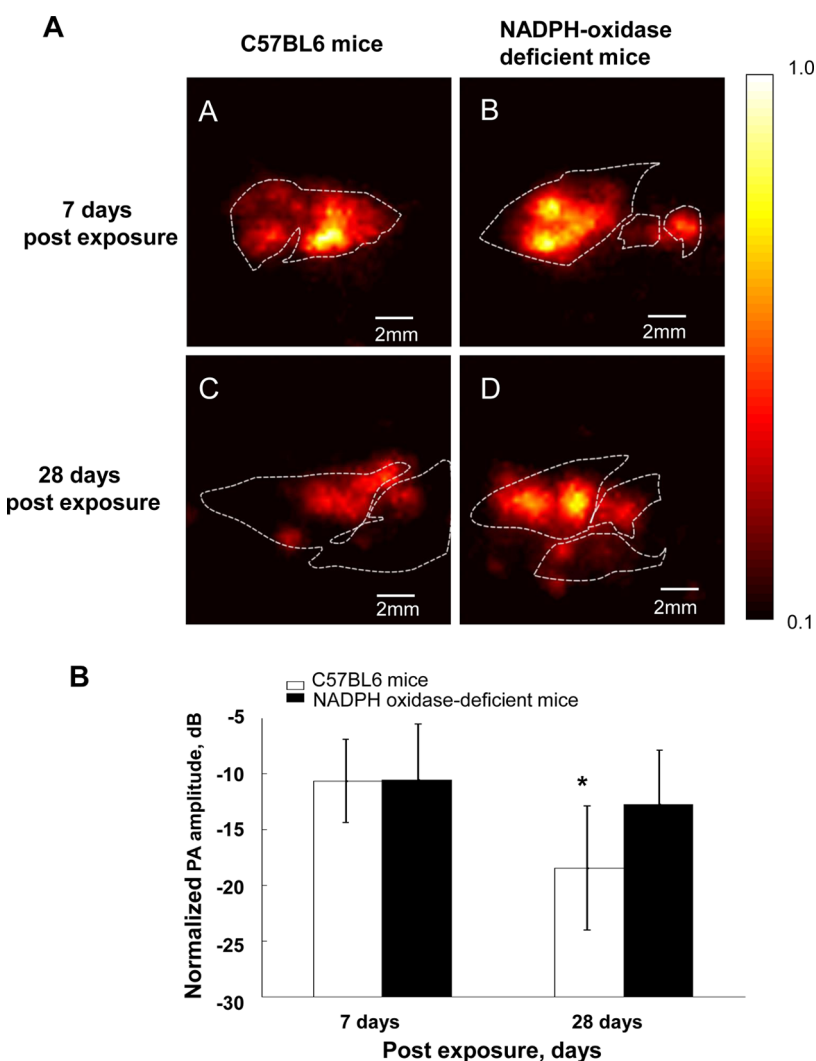


Figure 2. Photoacoustic (PA) images (A) and statistical analysis (B) of PA intensity of lung sections of adult C57BL/6 [$\text{gp91}^{\text{phox}(+/+)}\text{-}$] and NADPH-oxidase-deficient [$\text{gp91}^{\text{phox}(-/-)}$] mice on days 7 and 28 post SWCNT exposure. PA images were obtained by scanning over an area of 1.3 cm by 1.3 cm in 250 μm step increments. White dashed lines in each panel (A) depict the boundaries of the corresponding histology samples. PA signal intensity in each image was averaged over the areas within the white dashed lines and presented in dB (panel B). * $p < 0.001$, vs day 7 post SWCNT exposure.

fluorescent emission, which was dramatically enhanced by PMA activation (Figure 4A). Uptake of SWCNTs by activated THP-1 cells was accompanied by a marked decrease in HPF fluorescence emission intensity (Figure 4A), indicating that a significant part of peroxynitrite was interacting with SWCNTs rather than with HPF.

The difference between the fluorescence of naïve and PMA-activated THP-1 macrophages was assessed quantitatively using the Cellomics CellInsight HCS reader. PMA caused a 2.4-fold increase of HPF fluorescence compared with untreated cells (Figure 4B). The high level of fluorescence intensity of PMA-activated cells did not significantly change over 3 days, suggesting uninterrupted production of peroxynitrite by macrophages during this period of time. Results of consecutive measurements demonstrated a progressive increase in the fluorescence of HPF oxidation products in samples containing SWCNTs. Notably, the fluorescence intensity

did not reach the level observed in PMA-activated macrophages without SWCNTs.

Quenching of HPF oxidation products' fluorescence by SWCNTs could contribute to the observed reduction of fluorescence intensity. However, we found that exposure of PMA-activated THP-1 macrophages to a higher dose (two times) of SWCNTs (20 vs 10 μg) caused only an insignificant further change in the fluorescence response (Figure 4B). Moreover, in nonactivated THP-1 cells, SWCNTs (20 and 10 μg) did not affect the fluorescence response (Figure 4B inset b). These results are difficult to rationalize within the concept of nonspecific physical fluorescence quenching by SWCNTs. On the basis of these results, we suggested that a combined effect including both the competition of SWCNTs with HPF for peroxynitrite and quenching of HPF oxidation products' fluorescence by SWCNTs might account for the observed effect. Successful competition between

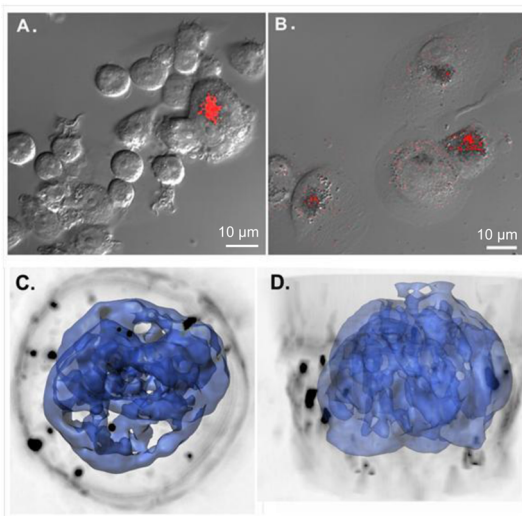


Figure 3. Representative images of THP-1 macrophage with SWCNT inclusions. Cells were cultured in RPMI 1640 media activated by overnight incubation with PMA ($50 \text{ pmol}/10^6$ cells). After 24 h, $20 \mu\text{g}$ of nanotubes was exposed to activated macrophages (10×10^6 cells in 2.5 mL of media) for a further 72 h at 37°C . (A) Differential interference contrast (DIC) microscopy in naive cells. Particles were extracted by threshold based on size, shape, and contrast and pseudocolored red. Cells that were nonactivated (as evidenced by cell flattening) were only rarely found to engulf SWCNTs as compared to PMA-activated cells in panel B, which avidly engulfed SWCNTs. (C) En face view of a 3D minimum intensity reconstruction of deconvolved wide-field image of PMA-activated cells containing SWCNTs (black). Nuclei are labeled blue (Hoescht). (D) Orthogonal view of the same reconstruction shown in panel C.

SWCNTs and HPF for peroxy nitrite can be rationalized based on comparison of “reacting concentrations” of the dye ($5 \mu\text{M}$) with equivalent molecular masses of SWCNTs (corresponding to $\sim 15 \text{ mM}$ of oxidizable carbons). The high content of oxidizable sites in SWCNTs may explain, at least in part, the quenching rate of the peroxy nitrite-dependent fluorescence response.

To further verify the ability of THP-1 cells to oxidatively degrade functionalized SWCNTs, we employed Raman microscopy. SWCNTs have two characteristic bands in Raman spectra: the tangential-mode G-band at $\sim 1580 \text{ cm}^{-1}$ and the disorder-induced D-band at $\sim 1340 \text{ cm}^{-1}$. Raman microscopy demonstrated a typical increase in the intensity of the D/G ratio after the incubation of SWCNTs with PMA-activated THP-1 cells (Figure 5A). Direct measurements of the SWCNT size distribution by TEM revealed a marked shift of the average SWCNT length from 1400 to 1800 nm (the full length range 400–2400 nm) to 400–1000 nm after 96 h of incubation with activated THP-1 cells (Figure 5B). These changes in SWCNT size were not observed after incubations with nonactivated macrophages.

Finally, we set out to use chemical models and test the ability of peroxy nitrite-generating systems to oxidatively biodegrade functionalized SWCNTs. Similarly to macrophage production of peroxy nitrite via

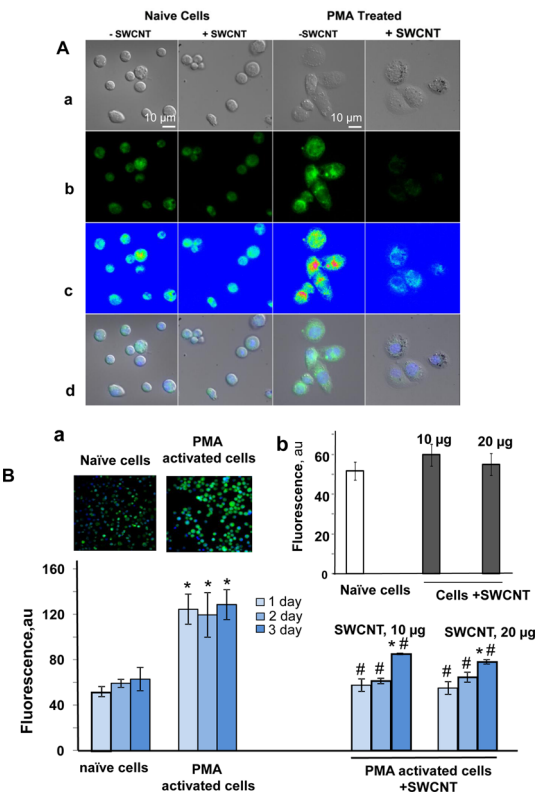


Figure 4. Assessment of peroxy nitrite production by THP-1 macrophages. Cells were cultured in RPMI 1640 media. A subset of cells was activated by overnight incubation with PMA ($50 \text{ pmol}/10^6$ cells). Cells were incubated with HBSS containing $5 \mu\text{M}$ hydroxyphenyl fluorescein (HPF) for 40 min. (A) Live cell imaging of HPF fluorescence in THP-1 cells. (a) DIC images, followed by the HPF emissions, first in green (b) and then pseudocolored based on emission intensity (c) to reveal subtle differences in intensity that may not be readily apparent in the original image. (d) Overlay of the DIC and fluorescent images (HPF, green; nuclei, blue). (B) Quantification of peroxy nitrite production by THP-1 macrophages using the Cellomics CellInsight HCS reader. Insets: (a) Typical images of naïve and PM-activated THP-1 macrophages incubated with HPF obtained using the Cellomics CellInsight HCS reader; (b) effect of SWCNTs on the intensity of peroxy nitrite-dependent fluorescence of HPF oxidation products by nonactivated THP-1 macrophages. * $p < 0.05$, vs naïve cells; # $p < 0.05$, vs PMA-activated cells.

reaction 1, we selected two systems to generate peroxy nitrite by either (i) combining a superoxide-generating system, xanthine oxidase/xanthine (XO/X), with NO* donors (PAPA-NONOate or spermine NONOate) or (ii) simultaneously producing superoxide and NO* by decomposition of SIN-1. In both of these systems, degradation of SWCNTs was detectable visually as the initially optically dense SWCNT suspensions were becoming more translucent over time (Figure 6A). To more objectively document SWCNT degradation, we used UV-vis-NIR spectroscopy. Typical UV-vis-NIR spectra of SWCNTs contained two characteristic absorption bands: the metallic band (M1) located in the area of 650–750 nm and the semiconducting transition band (S2) at 1000–1100 nm (Figure 6B inset a). As the graphitic structure becomes oxidized, transitions

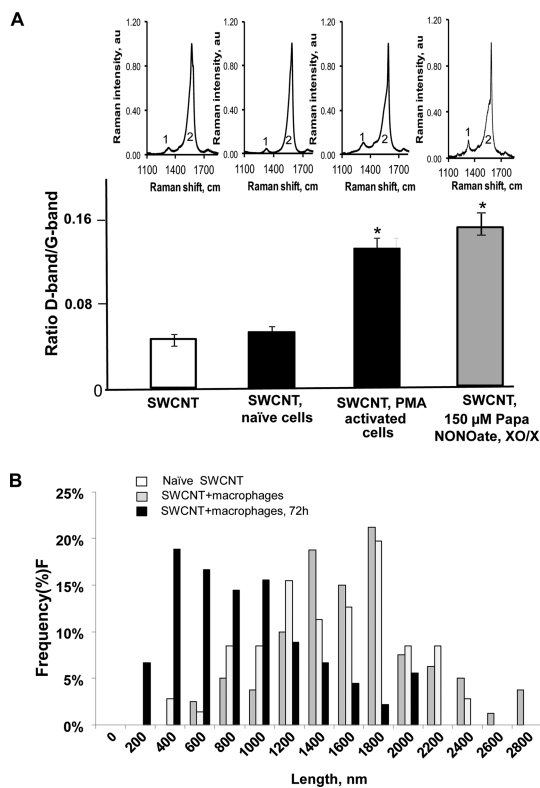


Figure 5. Raman spectra (A) and TEM (B) evaluation of SWCNT size distribution illustrating biodegradation of SWCNTs by THP-1 macrophages. 20 μg amount of SWCNTs was incubated with THP-1 cells activated by overnight incubation with PMA (10×10^6 cells in 2.5 mL of media) for 72 h. After collection of cells SDS was added to the cell pellets to a final concentration of 1%. Samples were heated at 100 $^\circ\text{C}$ for 15 min and sonicated using the ultrasonic benchtop cleaner (Branson 2510, output power of 70 W at 40 kHz) for 15 min. Finally, the material with 100 $\mu\text{g}/\text{mL}$ of proteinase K was incubated at 50 $^\circ\text{C}$ for 18 h.

associated with the sp^2 carbon framework of pristine SWCNTs diminished and finally completely disappeared. We detected that samples incubated in the presence of peroxynitrite-generating systems elicited a decrease of absorbance at the characteristic S2 band wavelength around 1075 nm (Figure 6B). Degradation of functionalized SWCNTs was dependent upon the amounts of peroxynitrite and was more effective with xanthine oxidase/xanthine + NO*-donors superoxide/NO \rightarrow ONOO⁻generating systems than with SIN-1. We performed time-course measurements of SWCNT degradation by PAPA NONOate plus XO/XO and Sin-1 (at the same concentration of 300 μM). We found that the half-life degradation times were \sim 50 h and more than 200 h, respectively (Figure 6B inset b).

SWCNTs are capable of inducing oxidative reactions due to the presence of adventitious transition metals.³⁴ Based on the XPS survey spectrum (Supporting Information, Figure S2), it appears that most metal residues (4–8 wt %) that remained in the commercial P2-SWNT were removed during the acid treatment process. Assessments of redox activity of SWCNT samples by

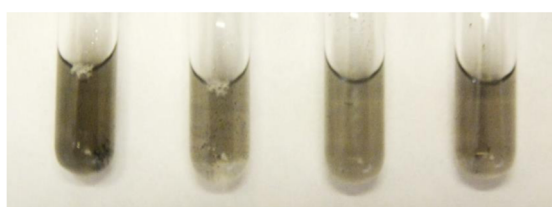
EPR spectroscopy demonstrated that they did not contain detectable signals from iron paramagnetic centers readily detectable by this technique in unpurified samples. On the basis of these characterizations we conclude that SWCNT degradation found in our experiments stemmed primarily from peroxynitrite-mediated oxidation.

Oxidative defects of SWCNTs induced by treatment with peroxynitrite generators were also detectable by Raman spectroscopy. A typical Raman spectrum registered from nonoxidized SWCNTs had a pronounced G-band and a very weak D-band (Figure 7A, inset). Incubation with peroxynitrite generators induced an increase of D-band, due to defects in sp^2 -hybridized carbon systems, and a decrease of the intensity of the tangential G mode, leading to the increased intensity of the D/G ratio (Figure 7A). Drastic changes in SWCNT morphology were demonstrated by TEM and SEM. After prolonged incubations in the presence of peroxynitrite-generating systems, the characteristic fibrillar structure of intact SWCNT was completely lost with simultaneous appearance of aggregated globular material (Figure 7B). These results were in agreement with our previous studies using HRP and MPO.¹¹

DISCUSSION

A number of studies have demonstrated that SWCNTs are capable of inducing a robust inflammatory response that can be synergistically enhanced by oxidative stress either produced *via* activation of the redox machinery of inflammatory cells (neutrophils and macrophages)^{35,36} or associated with the presence of adventitious transition metals.³⁴ Macrophages are viewed as the major type of inflammatory cells defining the fate of nanoparticles *via* their ability to take up, transport, and redistribute them in the body.^{1,37,38} Peroxynitrite serves as a macrophage-derived cytotoxic effector molecule to bacteria and parasites.^{39,40} The rate of peroxynitrite formation is increased many fold upon their activation: for rat alveolar macrophages activated with PMA, it was found to reach the level of \sim 100 pmol 10^6 cells⁻¹ min⁻¹.⁴¹ Here we demonstrated that carbonaceous nanoparticles may be taken up by macrophages and “oxidatively digested” by peroxynitrite generated in activated macrophages *via* NADPH-oxidase-driven production of superoxide anion radicals and NO*. It is also likely that clearance of CNTs from the lung might be due to the enhanced macrophage transport. Our *in vitro* experiments with THP-1 macrophages directly revealed their ability to oxidatively degrade SWCNTs in a process uncomplicated by possible clearance of SWCNTs from the lung due to the enhanced macrophage transport.

Our previous studies described the MPO-dependent biodegradation of SWCNTs in neutrophils.^{13,14} However, the neutrophilic cell response to SWCNTs is short-lived,^{19,20} and both “worn-out” neutrophils and their contents are engulfed and taken up by macrophages.⁴² In contrast, macrophages are recruited to the tissues for

A

SWCNT 150 μM
PAPA NONOate,
XO/XOX
150 μM
Spermine
NONOate,
XO/XOX,
300 μM
Sin-1

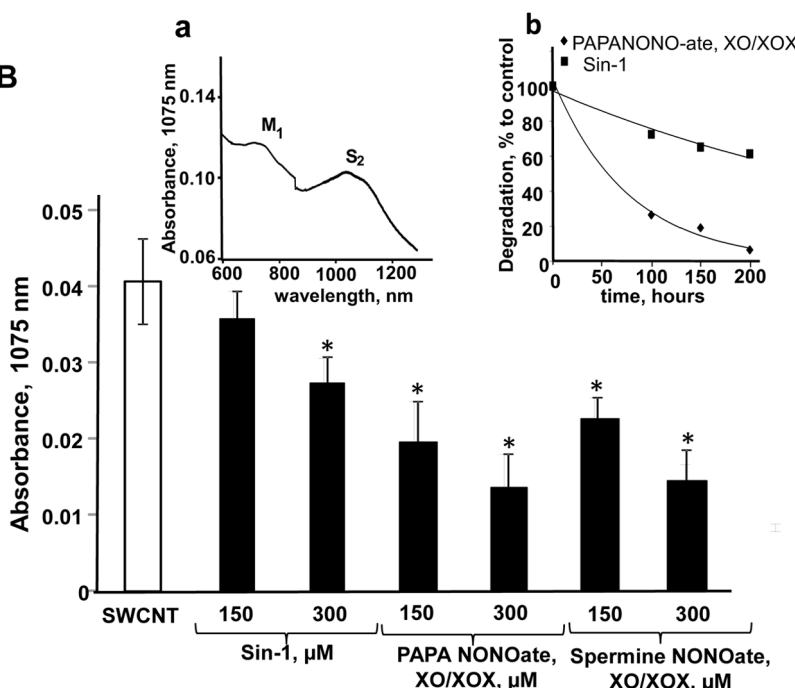
B

Figure 6. Visual and UV–vis–NIR absorption spectroscopic evaluation of peroxynitrite-mediated degradation of SWCNTs *in vitro*. SWCNTs (12 μg per sample) were incubated in 50 mM phosphate buffer (pH 7.4) with different peroxynitrite-generating compounds for 120 h at 37 °C. PAPA NONOate, spermine NONOate, SIN-1, and xanthine (final concentrations 150 or 300 μM) were added every 1.5 h, 5 times a day; 1.5 μL of solution contained 0.125 mU of xanthine oxidase was added in the morning and in the evening. (A) Visual evidence of peroxynitrite-mediated degradation of SWCNTs. (B) UV–vis–NIR absorption spectroscopic evaluation of peroxynitrite-mediated degradation of SWCNTs. Insets: (a) Typical UV–vis–NIR spectra of SWCNT; (b) degradation time-course of SWCNT incubated with peroxynitrite-generating systems: PAPA NONOate/XO/XOX and Sin-1 (at concentrations of 300 μM). * $p < 0.05$, vs control.

extended stay, thus providing sufficient time for the “oxidative digestion” of SWCNTs. One can envision that neutrophils may play a triggering role by initiating the SWCNT degradation process and converting longer particles into shorter ones, thus facilitating their uptake by one of several kinds of macrophages—the intravascular, interstitial, pleural, and surface—present in the lung.

Comparisons of redox potentials are quite useful for general assessments of potentially effective oxidants capable of, at least in principle, biodegrading CNTs. In fact, these comparisons turned out to be predictive of metal-driven oxidations of SWCNTs.⁴³ Similarly, several other potent oxidants—hydroxyl/hydroperoxyl radicals (2.33 V), reactive intermediates of peroxidases (~1.1 V), HOCl/HOBr (1.48 and 1.33 V, respectively), and peroxynitrite (1.4 V)—can all be viewed as

potential candidates for effective oxidative biodegradation of CNTs. These compounds can be reduced as acceptors of electrons from the valence band of CNTs, thus resulting in the oxidation of the latter. Recent work has demonstrated that SWCNTs can be biodegraded by exogenous and endogenous enzymes or by fluids mimicking the content of phagolysosomes.^{11,12} Within the context of the superoxide/peroxynitrite mechanism of SWCNT biodegradation, the acidic pH in the intraphagolysosomes may facilitate protonation of O-NOO to yield ONOOH. The latter can be more readily decomposed to hydroxyl radicals²⁴ with their known potential to directly oxidize SWCNTs.⁹

In contrast to MPO of neutrophils and eosinophil peroxidase of eosinophils—where reactive peroxidase intermediates, along with small molecules of hypohalogenous

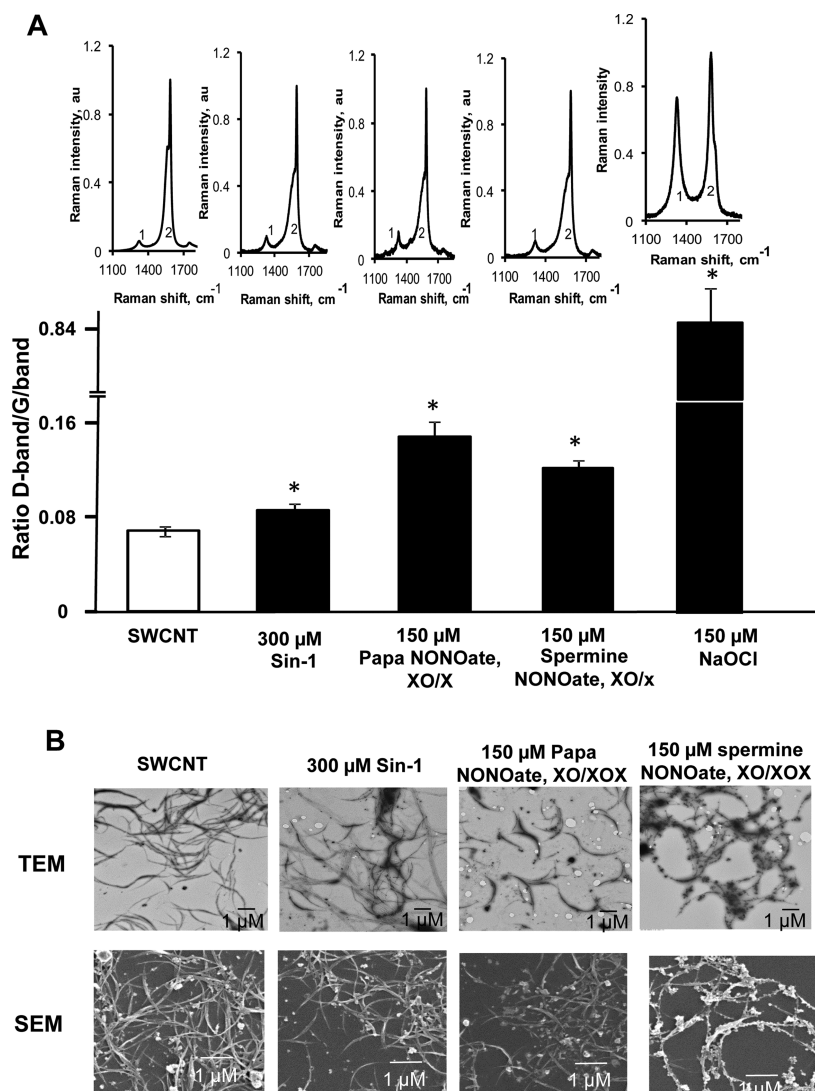


Figure 7. Raman spectra and TEM/SEM micrographs illustrating *in vitro* degradation of SWCNTs by peroxy nitrite. (A) D-band/G-band ratios for Raman spectra (excitation, 633 nm) of SWCNTs incubated with peroxy nitrite-generating compounds during 120 h. Treatment with NaOCl (150 μ M) was used as the positive control of degradation. Inset: Typical Raman spectra. (1) D-band, (2) G-band. * $p < 0.05$, vs control. (B) TEM (17 500 \times) and SEM (10 000 \times) images of SWCNTs illustrating changes of their morphology as a result of biodegradation in the presence of sources of peroxy nitrite *in vitro*.

acids, are involved in the biodegradation process—the macrophage superoxide/NO \rightarrow peroxy nitrite pathway does not include direct interactions of CNTs with the participating enzymes. As NADPH oxidase and NO synthase produce superoxide radicals and NO*, respectively, these two molecules react nonenzymatically at a diffusion-limited rate to yield peroxy nitrite.^{24,25} The latter can diffuse further to interact with CNTs. Thus, no specific protein/CNT binding is involved in oxidative biodegradation of carbon nanotubes. Our previous work demonstrated that enzymatic biodegradation realized via SWCNT interactions with reactive intermediates of peroxidases—horseradish peroxidase, myeloperoxidase, and eosinophil peroxidase—are more effective with oxidatively functionalized SWCNTs *vs* pristine SWCNTs, as negatively charged surfaces of the former can directly bind the positively charged

amino acid residues of the proteins, thus facilitating the catalytic process.^{13,44} However, this difference in the reactivity was detectable only when reactive enzymatic intermediates were involved in the biodegradation process⁹ and were negligible for the biodegradation process realized via HOCl-driven reactions.¹¹ Assuming that peroxy nitrite-dependent oxidations are also independent of the direct binding of reactive intermediates with the CNT surface, it is likely that superoxide/peroxy nitrite-driven oxidations by macrophages are also relatively insensitive to the initial oxidation state of CNTs. This may also be important for biomedical applications of CNTs in drug delivery paradigms: the indiscriminative attack by peroxy nitrite will likely not only affect the vehicle but also cause oxidative modification/degradation of the cargo, thus changing its therapeutic potential.

Our data on significantly less efficient clearance of oxidatively functionalized SWCNTs in the lung of NADPH-oxidase-deficient mice indicate that superoxide/NO* → peroxynitrite-driven reactions play a significant, albeit not exclusive, role in the biodegradation process. As NADPH-oxidase-deficient animals showed decreased capacity to "metabolize" SWCNTs, one may assume that there may be a genetically predetermined specificity in sensitivity to nanoparticle exposures. This may also relate to the expression of inducible NO synthase, a supplier of NO* as the second required reagent to produce peroxynitrite, directly involved in SWCNT degradation. Another group of factors may include expression of proteins engaged in engulfment and uptake of CNTs by macrophages. Our previous work⁴⁵ pointed to an anionic phospholipid, phosphatidylserine, as an "eat-me" signal facilitating the recognition and uptake of SWCNTs by macrophages. On the contrary, there are also "do not eat me" signals of protein nature that can be adsorbed on the CNT's surface, e.g., CD47, and suppress their uptake by macrophages,⁴⁶ hence slow down the biodegradation process.

The well-known claims of biopersistence and the ability to induce robust chronic inflammation have been stumbling blocks on the way to successful implementation of CNTs in biomedicine and have raised significant health concerns, particularly in environmental and occupational settings.^{4,47} Most of the relevant observations were published in the early days of the then emerging nanotoxicology, when adequate characterization of physicochemical characteristics of CNTs was not commonly performed. Consequently, the majority of this work has been conducted with very long, frequently entangled and aggregated into "bird's nests" CNT agglomerates.^{48,38} Later, it became apparent that the documented "biopersistence" of these high aspect ratio aggregated forms of SWCNTs was mainly due to their being surrounded by fibrous connective tissue in the lung with the formation of granulomas, isolating them from interactions with other cells including phagocytizing cells. As a result of this, SWCNTs present in granulomas may be less vulnerable to oxidative biodegradation mechanisms. In contrast, low aspect ratio SWCNTs are readily taken up by macrophages. Notably, nonaggregated low aspect ratio SWCNTs were found to be less toxic to macrophages than the aggregated forms.⁷

The identification of a new pathway for CNT biodegradation in macrophages raises a more general question on health risks as consequences of pulmonary exposure

to CNTs. While pharyngeal aspiration and inhalation of relatively high doses of SWCNTs have been clearly associated with robust inflammation, granulomas, and early onset fibrosis,^{20,36} the important issue is the relevance of these doses to realistic environmental and occupational levels of exposure. With the current very low levels of occupational exposures to CNTs at the workplace, estimated by NIOSH to be ~1 µg/m³,⁴⁹ it seems unlikely that low aspect ratio SWCNTs—with their effective biodegradation by neutrophil and macrophage oxidative pathways—may represent a significant health hazard. This evidently also applies to even lower levels of potential environmental exposures, hence leaving only accidental high levels of exposure to CNTs as a real risk.

CONCLUSIONS

Macrophages, in contrast to short-lived neutrophils, display persistent presence in the lung of animals after pulmonary exposure to carbon nanotubes. While effective in the clearance of bacterial pathogens and injured host cells, the ability of macrophages to "digest" carbonaceous nanoparticles has not been documented. Here, we used chemical, biochemical, and cell and animal models and demonstrated oxidative biodegradation of single-walled carbon nanotubes via superoxide/NO* → peroxynitrite-driven oxidative pathways of activated macrophages facilitating clearance of nanoparticles from the lung. Using two chemical models generating peroxynitrite, we visually detected degradation of SWCNTs, as the initially optically dense SWCNT suspensions were becoming more translucent over time. Additionally, CNT degradation by peroxynitrite was documented by (i) decreased absorbance at the semiconducting transition band at ~1075 nm, characteristic for SWCNTs, (ii) increased ratio of disorder-induced D-band to the tangential-mode G-band in Raman spectra, and (iii) decreased average SWCNT length assessed by electron microscopy. Activated THP-1 macrophages known to generate peroxynitrite upon stimulation with phorbol 12-myristate 13-acetate engulfed and biodegraded SWCNTs. Finally, significantly less efficient clearance of SWCNTs in the lung of NADPH-oxidase-deficient mice vs wild-type animals also indicated that superoxide/NO* → peroxynitrite-driven reactions play a significant, albeit not exclusive, role in the biodegradation process. Overall, we describe a superoxide/NO* → peroxynitrite-driven oxidative pathway in which macrophages are involved in "digestion" of CNTs and their clearance from the lung.

MATERIALS AND METHODS

Oxidation of SWCNTs. Approximately 10 mg of SWCNTs (P2, Carbon Solutions, Inc., Riverside, CA, USA) was sonicated (Branson 1510, frequency 40 kHz) in 20 mL of concentrated H₂SO₄/HNO₃ at

a ratio of 3:1 at 70 °C for 40 min. After diluting the solution 10-fold with deionized water, the oxidized SWCNTs were first filtered on a 0.22 µm Teflon membrane filter and subsequently washed with copious amounts of water until the pH of the filtrate was ~7.

The TEM was employed to determine the length distribution of the functionalized SWCNTs (Figure S1a). TEM and SEM images demonstrated that the acid mixture did not destroy the characteristic structure of carbon nanotubes. Raman spectroscopy was implemented to visualize the D- and G-bands (Figure S1b). Diffuse reflectance infrared Fourier transform spectroscopy was also performed (Supplemental Methods S1, Figure S1c). The surface chemistry of functionalized SWCNTs was evaluated by utilizing X-ray photoelectron spectroscopy (XPS). According to the description provided by Carbon Solution, Inc., the pristine P2-SWCNTs contain a carbonaceous content of over 90%. The XPS spectra (Supplementary Figure S2) belonging to P2 SWCNTs that were treated with a mixture of H_2SO_4 and HNO_3 (3:1) demonstrated that the oxygen content was markedly increased from less than 10% to an average of 30%. In addition, we listed the relative amounts of the different oxygen functional groups that were determined from the high-resolution spectra for both C 1s and O 1s. After sonication in the acid mixture, hydroxyl (or phenolic) groups were predominantly formed. Although present as minor functional groups, carboxylic acid/carboxylate groups were also found (Supplementary Figure S2). Additionally, we also measured the zeta potential and found that functionalization resulted in a more negative potential associated with the presence of carboxylic groups at a pH below 7.1.

Animals. Specific pathogen-free NADPH-oxidase-deficient [$gp91^{phox(-/-)}$] mice and adult C57BL/6 [$gp91^{phox(+/-)}$] mice (7–8 weeks old) were supplied by Jackson Laboratories (Bar Harbor, ME, USA). Animals were housed one mouse per cage in AAALAC-accredited NIOSH animal facilities 1 week prior to use. Beta Chips (Northeastern Products Corp., Warrensburg, NY, USA) were used for beddings and changed weekly. Animals were supplied with water and Teklad 7913 mouse/rat diet (Harlan, Indianapolis, IN, USA) *ad libitum*, in accordance with guidelines and policy set forth by the Institute of Laboratory Animals Resources, National Research Council. Experiments were conducted under a protocol approved by the Animal Care and Use Committee of NIOSH.

Quantitative Assessment of Alveolar Macrophages with SWCNTs. Alveolar macrophages with SWCNTs in lung sections from adult C57BL/6 [$gp91^{phox(+/-)}$] and NADPH-oxidase-deficient [$gp91^{phox(-/-)}$] mice were assessed using an enhanced dark-field optical system at days 7 and 28 postexposure. The lung sections stained with H&E were examined using dark-field-based illumination optics adapted to an Olympus BX-41 microscope (CytoViva, Auburn, AL, USA). The CytoViva system captures visible and near-infrared (400–1000 nm) spectra within each pixel of the scanned field with subsequent image analysis, comparing it with the characteristic spectrum of compounds of interest. Such an approach allows mapping and quantification of a wide range of nanomaterials inside cells and tissues.⁵⁰ Sections were inspected with 60 \times oil immersion objectives. The number of macrophages with SWCNTs was determined in the lung sections using a point counting overlay technique. An eyepiece counting overlay consisting of a grid with 126 lines (14 by 9 lines), each 1 cm in length and a total of 252 points for each throw of the overlay, was used. The grid pattern for throws of the counting overlay ensures a uniform sampling of the section that does not overweight interior points. The different sections of lung were imaged in an unbiased fashion by traversing the tissue in both the X and Y directions. At least 10 throws of the grid were counted per animal. The resulting values were expressed as a percentage of the total amount of alveolar macrophages.

Photoacoustic Imaging. The entire area of the sample submerged in a small water tank was illuminated by a pulsed laser light of 5 ns long at a repetition rate of 10 Hz, which was pumped by a Nd:YAG Q-switched pulsed laser (Brilliant, Quantel, France) and tuned to 680 nm in the optical parametric oscillator (Vibrant 532 HE I, OPOtek, CA, USA). A photoacoustic image was obtained by scanning over an area of 1.3 cm by 1.3 cm in 250 μm step increments, using a single-element focused ultrasound transducer (5 MHz, V 309-SU, Olympus NDT, MA, USA) mounted on a 2-axis translational stage (Zaber, Vancouver, Canada). The obtained PA signal intensity was normalized to the laser energy before applying a maximum

amplitude projection method to produce the normalized PA images. The Kruskal–Wallis nonparametric one-way test was applied to compare PA signal intensities.

Incubation of SWCNTs with Macrophages. The THP-1 human monocytic cell line obtained from American Tissue Culture Collections (ATCC) was maintained in RPMI 1640 culture media supplemented with 10% heat-inactivated FBS. Before the experiment cells were seeded in RPMI 1640 media without phenol red, and differentiation was activated by overnight incubation with PMA (50 pmol/10 6 cells). The next day 20 μg of nanotubes was exposed to activated macrophages (10 \times 10 6 cells in 2.5 mL of media) during 72 h at 37 °C. Then incubation media was removed, and cells were washed with phosphate-buffered saline (PBS) and trypsinized. The trypsin solution containing detached cells was combined with preliminary removed incubation media and PBS and centrifuged at 1200g for 20 min. Supernatant was removed, pellets were suspended in PBS, and 10% SDS was added to a final concentration of 1%. Samples were heated at 100 °C for 15 min and sonicated using the ultrasonic benchtop cleaner (Bransonic 2510, output power of 70 W at 40 kHz) for 15 min. Obtained samples were stored at –20 °C and used for assessment of SWCNT degradation by Raman spectroscopy and transmission electron microscopy (TEM). In control samples collecting of cells was started immediately after addition of SWCNTs.

Live Cell Imaging. Cells were seeded on 35 mm glass-bottom dishes (MatTek Corporation, Ashland, MA, USA) and incubated with the peroxynitrite indicator hydroxyphenyl fluorescein (HPF) (5 μM , Invitrogen, Eugene, OR, USA) for 15 min at 37 °C. Cells were washed with PBS, the media replaced, and the dish inserted in a closed, thermocontrolled (37 °C) stage top incubator (Tokai Hit Co., Shizuoka-ken, Japan) atop the motorized stage of an inverted Nikon TiE fluorescent microscope (Nikon Inc., Melville, NY, USA) equipped with a 60 \times oil immersion optic (Nikon, CFI PlanFluor, NA 1.43) and NIS Elements Software. HPF was excited using a Lumencor diode-pumped light engine (SpectraX, Lumencor Inc., Beaverton OR, USA) and detected using an FITC long pass filter set (Chroma Technology Corp, USA) and ORCA-Flash4.0 sCMOS camera (Hamamatsu Corporation, Bridgewater, NJ, USA). The number of SWCNTs per cell was quantified using the spots function in NIS Elements (Nikon Inc.).

Measurement of Peroxynitrite Production by THP-1 Cells. Detection of peroxynitrite produced by THP-1 macrophages was done using HPF. Briefly cells were suspended in RPMI 1640 media without phenol red and seeded in a 96-well plate (10 \times 10 3 cells/well in a volume of 100 μL), and part of cells were incubated overnight with PMA (50 pmol/10 6 cells) to activate differentiation. Measurements were done during 3 days after incubation of cells with PMA. Every day staining was performed using new unstained wells containing THP-1 cells and a freshly prepared solution of HPF in Hank's balanced salt solution (HBSS). Before measurement cells were washed two times with 150 μL of HBSS and incubated with HBSS containing 5 μM HPF for 40 min. In some cases before incubation with HPF cells were labeled with Hoechst 33342 in a final concentration of 1 $\mu g/mL$ for 15 min. Images were analyzed using the Cellomics CellInsight HCS reader (Thermo Scientific, Waltham, MA, USA) and multichannel high content screening BioApplication software (Compartmental Analysis). Seventy-five fields were analyzed per each well.

Incubation of SWCNTs with Peroxynitrite *In Vitro*. SWCNTs (9 μg per sample) were incubated in 50 mM phosphate buffer (pH 7.4) with different concentrations of peroxynitrite for 120 h at 37 °C. Peroxynitrite was generated (a) by addition of peroxynitrite donor SIN-1, producing both nitric oxide (4NO) and superoxide ($^{\bullet}O_2^-$) upon decomposition in aqueous solution, or (b) by simultaneous addition of a superoxide-generating system, containing xanthine oxidase/xanthine (XO/X) and a NO donor (PAPA NONOate or spermine NONOate), spontaneously dissociating and liberating 2 mol of NO per mole of parent compound. Aliquots of fresh PAPA NONOate, spermine NONOate, xanthine, and SIN-1 (final concentrations of 150 or 300 μM) were added every 1.5 h (5 times a day); 1.5 μL of solution contained 0.125 mU of xanthine oxidase was added in the morning and in the evening.

Preparation of Samples for Transmission and Scanning Electron Microscopy and Raman Spectroscopy. SDS (1%) was added to SWCNT samples containing cellular material, and the mixtures were heated to 100 °C for 10 min. This was followed by sonication using the ultrasonic benchtop cleaner (Branson 2510, output power of 70 W at 40 kHz) for 10 min. After cooling the contents to room temperature, Tris-HCl buffer (final concentration 30 mM) (pH 8.0) was added. Finally, an 18 h incubation of the material with 100 µg/mL of proteinase K at 50 °C was undertaken. After these treatments, most of the cell contents were removed from the samples, resulting in SWCNT pellets well prepared for the analysis by TEM and Raman spectroscopy. No cell remnants were detectable on TEM pictures of the samples. Raman spectra of the samples looked similar to those of SWCNT suspensions.

Transmission Electron Microscopy. A 5 µL amount of solubilized sample was placed on a lacey carbon grid (Pacific-Grid Tech, San Francisco, CA, USA) and permitted to dry overnight under ambient conditions prior to TEM imaging (FEI Morgagni, 80 keV, Hillsboro, OR, USA). Finally, ImageJ was employed to measure the length of the nanotubes.

Scanning Electron Microscopy. A 10 µL portion of sonicated sample was placed on a coverslip and allowed to dry. Then samples were mounted on an aluminum stub and sputter coated with 3.5 nm of gold palladium, and SEM examination was made with a Jeol JSM-6335F SEM.

Raman Spectroscopy. Samples were prepared by drop-casting approximately 30 µL of solubilized material on a microscope slide and allowed to dry. A Renishaw inVia Raman microscope spectrometer (Renishaw, Gloucestershire, UK) with an excitation wavelength of 633 nm was used for all samples. Spectra were obtained over the range 1000 to 1800 cm⁻¹ to visualize D- and G-band intensity changes throughout the degradation process. Spectra were collected with a 15 s exposure time, at 50% laser power, and averaged across three scans per sample.

Ultraviolet–Visible–Near-Infrared Absorption Spectroscopy. The vis–NIR spectra were obtained from the samples using a PerkinElmer Lambda 750 UV/vis/NIR spectrophotometer (PerkinElmer, Waltham, MA, USA). Spectra were recorded using a 50 µL cuvette (Starna Cell Inc., Atascadero, CA, USA). Absorbance in the region of the S2 band was normalized by subtraction of scattering.

Statistics. The results are presented as mean ± SD values from three experiments, and statistical analyses were performed using Student's *t* test. The statistical significance of differences was set at *p* < 0.05.

Disclosure: The findings and conclusions in this report are those of the authors and do not necessarily represent the views of the National Institute for Occupational Safety and Health.

Conflict of Interest: The authors declare no competing financial interest.

Acknowledgment. This work was supported by the National Institute for Occupational Safety and Health (NIOSH), OH008282, and National Institutes of Health, NIEHS R01ES019304, U19AI068021, PO1HL114453, and RFBR 12-04-01293. G.P.K. acknowledges an EPA STAR Graduate Fellowship, FP-91713801.

Supporting Information Available: Characterization of SWCNTs employed in the study, supporting information, and methods. This material is available free of charge via the Internet at <http://pubs.acs.org>.

REFERENCES AND NOTES

- Sanchez, V. C.; Pietruska, J. R.; Miselis, N. R.; Hurt, R. H.; Kane, A. B. Biopersistence and Potential Adverse Health Impacts of Fibrous Nanomaterials: What Have We Learned from Asbestos? *Wiley Interdiscip. Rev.: Nanomed. Nanobiotechnol.* **2009**, 1 (5), 511–529.
- Xia, T.; Li, N.; Nel, A. E. Potential Health Impact of Nanoparticles. *Annu. Rev. Public Health* **2009**, 30, 137–150.
- Ishimatsu, S.; Hori, H.; Kasai, T.; Ogami, A.; Morimoto, Y.; Oyabu, T.; Tanaka, I. Biological Effect of Carbon Graphite Whisker in Rat Lung by Long-Term Inhalation. *Inhal. Toxicol.* **2009**, 21, 668–673.
- Shvedova, A. A.; Kagan, V. E. The Role of Nanotoxicology in Realizing the 'Helping Without Harm' Paradigm of Nanomedicine: Lessons from Studies of Pulmonary Effects of Single-Walled Carbon Nanotubes. *J. Int. Med.* **2010**, 267, 106–118.
- Jain, S.; Thakare, V. S.; Das, M.; Godugu, C.; Jain, A. K.; Mathur, R.; Chuttani, K.; Mishra, A. K. Toxicity of Multiwalled Carbon Nanotubes with End Defects Critically Depends on Their Functionalization Density. *Chem. Res. Toxicol.* **2011**, 24, 2028–2039.
- Kolosnjaj-Tabi, J.; Hartman, K. B.; Boudjemaa, S.; Ananta, J. S.; Morgan, G.; Szwarc, H.; Wilson, L. J.; Moussa, F. In Vivo Behavior of Large Doses of Ultrashort and Full-Length Single-Walled Carbon Nanotubes after Oral and Intraperitoneal Administration to Swiss Mice. *ACS Nano* **2010**, 4, 1481–1492.
- Porter, A. E.; Gass, M.; Bendall, J. S.; Muller, K.; Goode, A.; Skepper, J. N.; Midgley, P. A.; Welland, M. Uptake of Noncytotoxic Acid-Treated Single-Walled Carbon Nanotubes into the Cytoplasm of Human Macrophage Cells. *ACS Nano* **2009**, 3, 1485–1492.
- Wei, Z. H.; Wang, H.; Chen, X. Y.; Wang, B. S.; Rong, Z. X.; Wang, B. S.; Su, B. H.; Chen, H. Z. Time-and Dose-Dependent Effect of Psyllium on Serum Lipids in Mild-To-Moderate Hypercholesterolemia: A Meta-Analysis Of Controlled Clinical Trials. *Eur. J. Clin. Nutr.* **2009**, 63, 821–827.
- Allen, B. L.; Kotchey, G. P.; Chen, Y.; Yanamala, N. V.; Klein-Seetharaman, J.; Kagan, V. E.; Star, A. Mechanistic Investigations Of Horseradish Peroxidase-Catalyzed Degradation of Single-Walled Carbon Nanotubes. *J. Am. Chem. Soc.* **2009**, 131, 17194–17205.
- Naqui, A.; Chance, B.; Cadena, E. Reactive Oxygen Intermediates in Biochemistry. *Annu. Rev. Biochem.* **1986**, 55, 137–166.
- Kotchey, G. P.; Hasan, S. A.; Kapralov, A. A.; Ha, S. H.; Kim, K.; Shvedova, A. A.; Kagan, V. E.; Star, A. A Natural Vanishing Act: The Enzyme-Catalyzed Degradation of Carbon Nanomaterials. *Acc. Chem. Res.* **2012**, 45, 1770–1781.
- Russier, J.; Menard-Moyon, C.; Venturelli, E.; Gravel, E.; Marcolongo, G.; Meneghetti, M.; Doris, E.; Bianco, A. Oxidative Biodegradation of Single- and Multi-Walled Carbon Nanotubes. *Nanoscale* **2011**, 3, 893–896.
- Kagan, V. E.; Konduru, N. V.; Feng, W.; Allen, B. L.; Conroy, J.; Volkov, Y.; Vlasova, I. I.; Belikova, N. A.; Yanamala, N.; Kapralov, A.; et al. Carbon Nanotubes Degraded by Neutrophil Myeloperoxidase Induce Less Pulmonary Inflammation. *Nat. Nanotechnol.* **2010**, 5, 354–359.
- Shvedova, A. A.; Kapralov, A. A.; Feng, W. H.; Kisin, E. R.; Murray, A. R.; Mercer, R. R.; St Croix, C. M.; Lang, M. A.; Watkins, S. C.; Konduru, N. V.; et al. Impaired Clearance and Enhanced Pulmonary Inflammatory/Fibrotic Response to Carbon Nanotubes in Myeloperoxidase-Deficient Mice. *PloS One* **2012**, 7, e30923.
- Furtmuller, P. G.; Zederbauer, M.; Jantschko, W.; Helm, J.; Bogner, M.; Jakobitsch, C.; Obinger, C. Active Site Structure and Catalytic Mechanisms of Human Peroxidases. *Arch. Biochem. Biophys.* **2006**, 445, 199–213.
- Arnhold, J.; Flemming, J. Human Myeloperoxidase in Innate and Acquired Immunity. *Arch. Biochem. Biophys.* **2010**, 500, 92–106.
- Yoon, S. M.; Kim, S. J.; Shin, H. J.; Benayad, A.; Choi, S. J.; Kim, K. K.; Kim, S. M.; Park, Y. J.; Kim, G.; Choi, J. Y.; et al. Selective Oxidation on Metallic Carbon Nanotubes by Halogen Oxoanions. *J. Am. Chem. Soc.* **2008**, 130 (8), 2610–2616.
- Zhang, L.; Petersen, E. J.; Habteselassie, M. Y.; Mao, L.; Huang, Q. Degradation of Multiwall Carbon Nanotubes by Bacteria. *Environ. Pollut.* **2013**, 181, 335–339.
- Soehnlein, O.; Lindbom, L.; Weber, C. Mechanisms Underlying Neutrophil-Mediated Monocyte Recruitment. *Blood* **2009**, 114 (21), 4613–4623.
- Shvedova, A. A.; Kisin, E.; Murray, A. R.; Johnson, V. J.; Gorelik, O.; Arepalli, S.; Hubbs, A. F.; Mercer, R. R.; Keohavong, P.; Sussman, N.; et al. Inhalation vs. Aspiration Of Single-Walled Carbon Nanotubes in C57BL/6 Mice: Inflammation,

- Fibrosis, Oxidative Stress, and Mutagenesis. *Am. J. Physiol. Lung Cell. Mol. Physiol.* **2008**, *295*, L552–L565.
21. Dale, D. C.; Boxer, L.; Liles, W. C. The Phagocytes: Neutrophils and Monocytes. *Blood* **2008**, *112*, 935–945.
 22. Linares, E.; Giorgio, S.; Mortara, R. A.; Santos, C. X.; Yamada, A. T.; Augusto, O. Role of Peroxynitrite in Macrophage Microbicidal Mechanisms *In Vivo* Revealed by Protein Nitration and Hydroxylation. *Free Radical Biol. Med.* **2001**, *30*, 1234–1242.
 23. Forman, H. J.; Torres, M. Redox Signaling in Macrophages. *Mol. Aspects Med.* **2001**, *22*, 189–216.
 24. Szabo, C.; Ischiropoulos, H.; Radi, R. Peroxynitrite: Biochemistry, Pathophysiology and Development of Therapeutics. *Nat. Rev. Drug Discovery* **2007**, *6*, 662–680.
 25. Pacher, P.; Beckman, J. S.; Liaudet, L. Nitric Oxide and Peroxynitrite in Health and Disease. *Physiol. Rev.* **2007**, *87*, 315–424.
 26. Shvedova, A. A.; Kisin, E. R.; Murray, A. R.; Kommineni, C.; Castranova, V.; Fadel, B.; Kagan, V. E. Increased Accumulation of Neutrophils and Decreased Fibrosis in the Lung of NADPH Oxidase-Deficient C57BL/6 Mice Exposed to Carbon Nanotubes. *Toxicol. Appl. Pharmacol.* **2008**, *231*, 235–240.
 27. Badireddy, A. R.; Wiesner, M. R.; Liu, J. Detection, Characterization, and Abundance of Engineered Nanoparticles in Complex Waters by Hyperspectral Imagery with Enhanced Darkfield Microscopy. *Environ. Sci. Technol.* **2012**, *46*, 10081–10088.
 28. Weintraub, H.; Brehm-Stecher, B. F. Enhanced Dark Field Microscopy for Rapid Artifact-Free Detection of Nanoparticle Binding to *Candida Albicans* Cells and Hyphae. *Biotechnol. J.* **2009**, *4*, 871–879.
 29. Koppenol, W. H.; Moreno, J. J.; Pryor, W. A.; Ischiropoulos, H.; Beckman, J. S. Peroxynitrite, a Cloaked Oxidant Formed by Nitric Oxide and Superoxide. *Chem. Res. Toxicol.* **1992**, *5*, 834–842.
 30. Kim, K. H. S. W.; Ashkenazi, S.; O'Donnell, M.; Agarwal, A.; Kotov, N. A.; Denny, M. F.; Kaplan, M. J. Photoacoustic Imaging of Early Inflammatory Response Using Gold Nanorods. *Appl. Phys. Lett.* **2007**, *90*, 223901–223903.
 31. Bielski, B. H. J.; Cabelli, D. E.; Arudi, R. L.; Ross, A. B. Reactivity of HO₂/O₂⁻ Radicals in Aqueous Solution. *J. Phys. Chem. Ref. Data* **1985**, *14*, 1041–1110.
 32. Qin, Z. The Use Of THP-1 Cells as a Model for Mimicking the Function and Regulation of Monocytes and Macrophages in the Vasculature. *Atherosclerosis* **2012**, *221*, 2–11.
 33. Wardman, P. Fluorescent and Luminescent Probes for Measurement of Oxidative and Nitrosative Species in Cells and Tissues: Progress, Pitfalls, and Prospects. *Free Radical Biol. Med.* **2007**, *43*, 995–1022.
 34. Shvedova, A. A.; Pietrojost, A.; Fadel, B.; Kagan, V. E. Mechanisms of Carbon Nanotube-Induced Toxicity: Focus on Oxidative Stress. *Toxicol. Appl. Pharmacol.* **2012**, *261* (2), 121–133.
 35. Oberdorster, G. Nanotoxicology: *In Vitro-in Vivo* Dosimetry. *Environ. Health Perspect.* **2012**, *120*, A13author reply A13.
 36. Shvedova, A. A.; Kisin, E. R.; Mercer, R.; Murray, A. R.; Johnson, V. J.; Potapovich, A. I.; Tyurina, Y. Y.; Gorelik, O.; Arepalli, S.; Schwegler-Berry, D.; et al. Unusual Inflammatory and Fibrogenic Pulmonary Responses to Single-Walled Carbon Nanotubes in Mice. *Am. J. Physiol. Lung Cell. Mol. Physiol.* **2005**, *289*, L698–L708.
 37. Bussy, C.; Cambédouzou, J.; Lanone, S.; Leccia, E.; Hersanu, V.; Pinault, M.; Mayne-L'hermite, M.; Brun, N.; Mory, C.; Cotte, M.; et al. Carbon Nanotubes in Macrophages: Imaging and Chemical Analysis by X-Ray Fluorescence Microscopy. *Nano Lett.* **2008**, *8*, 2659–2663.
 38. Murphy, F. A.; Schinwald, A.; Poland, C. A.; Donaldson, K. The Mechanism of Pleural Inflammation by Long Carbon Nanotubes: Interaction of Long Fibres with Macrophages Stimulates Them to Amplify Pro-Inflammatory Responses in Mesothelial Cells. *Part. Fibre Toxicol.* **2012**, *9*, 8.
 39. Hickman-Davis, J. M.; O'Reilly, P.; Davis, I. C.; Peti-Peterdi, J.; Davis, G.; Young, K. R.; Devlin, R. B.; Matalon, S. Killing of Klebsiella pneumoniae by Human Alveolar Macrophages. *Am. J. Physiol. Lung Cell. Mol. Physiol.* **2002**, *282*, L944–L956.
 40. Darrah, P. A.; Hondalus, M. K.; Chen, Q.; Ischiropoulos, H.; Mosser, D. M. Cooperation Between Reactive Oxygen and Nitrogen Intermediates in Killing of *Rhodococcus Equi* by Activated Macrophages. *Infect. Immun.* **2000**, *68*, 3587–3593.
 41. Ischiropoulos, H.; Zhu, L.; Beckman, J. S. Peroxynitrite Formation from Macrophage-Derived Nitric Oxide. *Arch. Biochem. Biophys.* **1992**, *298*, 446–451.
 42. Cox, G.; Crossley, J.; Xing, Z. Macrophage Engulfment of Apoptotic Neutrophils Contributes to the Resolution of Acute Pulmonary Inflammation *In Vivo*. *Am. J. Respir. Cell Mol. Biol.* **1995**, *12*, 232–237.
 43. Choi, H. C.; Shim, M.; Bangsaruntip, S.; Dai, H. Spontaneous Reduction of Metal Ions on the Sidewalls of Carbon Nanotubes. *J. Am. Chem. Soc.* **2002**, *124*, 9058–9059.
 44. Andon, F. T.; Kapralov, A. A.; Yanamala, N.; Feng, W.; Baygan, A.; Chambers, B. J.; Hultenby, K.; Ye, F.; Toprak, M. S.; Brandner, B. D.; et al. Biodegradation of Single-Walled Carbon Nanotubes by Eosinophil Peroxidase. *Small* **2013**, *9*, 2721–2729.
 45. Konduru, N. V.; Tyurina, Y. Y.; Feng, W.; Basova, L. V.; Belikova, N. A.; Bayir, H.; Clark, K.; Rubin, M.; Stoltz, D.; Vallhov, H.; et al. Phosphatidylserine Targets Single-Walled Carbon Nanotubes to Professional Phagocytes *In Vitro* and *In Vivo*. *PLoS One* **2009**, *4*, e4398.
 46. Rodriguez, P. L.; Harada, T.; Christian, D. A.; Pantano, D. A.; Tsai, R. K.; Discher, D. E. Minimal "Self" Peptides that Inhibit Phagocytic Clearance and Enhance Delivery of Nanoparticles. *Science* **2013**, *339*, 971–975.
 47. Shvedova, A. A.; Kisin, E. R.; Porter, D.; Schulte, P.; Kagan, V. E.; Fadel, B.; Castranova, V. Mechanisms of Pulmonary Toxicity and Medical Applications of Carbon Nanotubes: Two Faces of Janus? *Pharmacol. Ther.* **2009**, *121*, 192–204.
 48. Donaldson, K.; P. C.; Murphy, F. A.; Macfarlane, M.; Chernova, T.; Schinwald, A. Pulmonary Toxicity of Carbon Nanotubes and Asbestos - Similarities and Differences. *Adv. Drug Delivery Rev.* **2013**, *65*, 2078–2086.
 49. Occupational Exposure to Carbon Nanotubes and Nanofibers. NIOSH Current Intelligence Bulletin No. 65, available online at <http://www.cdc.gov/niosh/docs/2013-145/pdfs/2013-145.pdf>, 2013.
 50. von der Kammer, F.; Ferguson, P. L.; Holden, P. A.; Masion, A.; Rogers, K. R.; Klaine, S. J.; Koelmans, A. A.; Horne, N.; Urine, J. M. Analysis of Engineered Nanomaterials in Complex Matrices (Environment and Biota): General Considerations and Conceptual Case Studies. *Environ. Toxicol. Chem.* **2012**, *31*, 32–49.